2mip

X-660
PREI

H^2, H^3, HE^3 PRODUCTION IN SOLAR FLARES

R. RAMATY
B. KOZLOVSKY

APRIL 1974

GSFC — GODDARD SPACE FLIGHT CENTER —
GREENBELT, MARYLAND

For information concerning availability of this document contact:

Technical Information Division, Code 250
Goddard Space Flight Center
Greenbelt, Maryland 20771

(Telephone 301-982-4488)

ii

H^2, H^3 and He^3 Production in Solar Flares

R. Ramaty and B. Kozlovsky*
Laboratory for High Energy Astrophysics
Goddard Space Flight Center
Greenbelt, Maryland 20771

*NAS/NRC Resident Research Associate on leave from
Tel Aviv University

Abstract

We evaluate in detail the production of deuterium, tritium, and helium-3 from nuclear reactions of accelerated charged particles with the ambient solar atmosphere. We use updated cross sections and kinematics, we extend our calculations to very low energies ($\sim$ 0.1 MeV/nucleon), and we calculate the angular distribution of the secondary particles. We then compare the calculations with data on accelerated isotopes from solar flares. In particular, we consider the August 1972 events for which both He^3 and nuclear gamma-rays were observed. Finally, we provide an explanation for He^3-rich events in terms of the angular distributions of secondary isotopes, and we make predictions on the flux of 2.2 MeV gamma rays from such flares.

I. Introduction

The isotopes H^2, H^3 and He^3 were detected in solar cosmic rays with abundances much larger than the H^2 and He^3 abundances or upper limits in both the solar wind and the photosphere (for summary of observational data see Section IV). Therefore, it is generally believed that energetic H^2, H^3 and He^3 from solar flares are produced mainly by nuclear reactions of accelerated H^1 and He^4 with the ambient material in the flare region. The principal difficulty with this interpretation, however, appears to be caused by observations of flare associated events with very large He^3/He^4 ratios, but which do not show detectable H^2 and H^3 fluxes (Garrard, Stone and Vogt 1973, Anglin 1974). In order to understand this apparent discrepancy in the context of all the available information on nuclear reactions in flares (both isotopic and gamma-ray data), we have reexamined in detail the production of H^2, H^3 and He^3 by accelerated particles, and we have compared our results with these data.

Previous detailed calculations on H and He isotope production and applications to galactic cosmic rays were done by Ramaty and Lingenfelter (1969) and by Meyer (1971, 1972). In the present paper we apply these calculations to solar flares. We also extend their treatments of the nuclear physics as follows: We calculate the secondary spectra down to very low energies (~ 0.1 MeV/nucleon), and we derive angular distributions for the isotopes; we supplement the cross sectional data on pCNO reactions at low energies; and we consider the destruction of the isotopes (in particular tritium) by nuclear reactions. The contributions of pCNO reactions, however, turns out to be unimportant for most cases of interest.

Isotope production in solar flares without consideration of reaction kinematics was previously treated by Lingenfelter and Ramaty (1967).

We then compare our results with data. For the flares of August 1972 for which both He^3 and nuclear gamma rays were observed (Webber 1974; Chupp et al. 1973), the isotope data implies that the product of the interaction time of the particles and the density of the ambient medium was about 4×10^{13} $cm^{-3}s$; this corresponds to a matter traversal for relativistic particles of ~ 2 gcm^{-2}. A similar matter traversal (~ 1 gcm^{-2}) is required to account for the deuterium and tritium observations from other flares. The He^3 observations from He^3-rich flares, however, require a much larger path length (>10 gcm^{-2}); moreover, because of the absence of H^2 and H^3, these events cannot be understood in terms of isotropic nuclear interactions in flares. We show that if the primary particles are directed downwards toward the Sun, the depletion of H^2 and H^3 could result from the preferential emission of these isotopes into the forward hemisphere, and from the destruction of H^3 by nuclear interactions. We expect such anisotropies mainly for small flares.

The validity of our model for He^3-rich flares could be checked by gamma-ray observations. Our prediction is that these flares should produce a time-integrated 2.2 MeV flux of about 3 photons cm^{-2}. We note, however, this value is quite uncertain, mainly because of uncertainties in the evaluation of the total number of He^3 nuclei released from the flare.

II. Isotope Production

The principal deuteron, triton and helium-3 producing reactions in proton-hydrogen (pp), proton-helium ($p\alpha$) and alpha-particle-hydrogen (αp) interactions are listed in Table 1. We also give the reaction thresholds and minimum secondary particle energies, $E_s(min)$ (Ramaty and Lingenfelter 1969). In addition to these reactions we consider interactions of accelerated protons with ambient CNO, and the interactions of accelerated CNO particles with ambient hydrogen. We have neglected $\alpha\alpha$ reactions, because no reliable data on cross sections exists for these reactions. We note, however, that by using approximate cross sections, Ramaty and Lingenfelter (1969) found that $\alpha\alpha$ reactions do not contribute appreciably to the total H^2 and He^3 production by galactic cosmic rays. In solar flares the contribution of $\alpha\alpha$ reactions will be even less, because here the ratio of accelerated alpha particles to accelerated protons is smaller than in the cosmic rays.

For the composition of the ambient solar atmosphere we use H:He:C:N:O = 1:0.07: 3.7×10^{-4}: 1.2×10^{-4}: 6.8×10^{-4} (Cameron 1973). For the accelerated particle populations we assume both power-law and exponential spectra, i.e.

$$N_i(E) = k_i E^{-S} \tag{1}$$

and

$$N_i(P) = k_i \exp(-P/Po), \tag{2}$$

respectively. Here $N_i(E)$ and $N_i(P)$ are the number of accelerated particles of kind i in the flare region per unit energy per nucleon, E, or unit rigidity, P; the k_i's are constants determined by normalizing

the N_i's to 1 proton of energy greater than 30 MeV, and by using the composition of the ambient solar atmosphere; and s and Po are, respectively, the spectral index and characteristic rigidity assumed to be the same for all accelerated particle components.

For isotope production in pα reactions we use the cross sections of Meyer (1972). For H^2 and H^3 production in pCNO reactions, and for He^3 production in pCNO reactions above about 20 MeV/nucleon we use the cross sections of Ramaty and Lingenfelter (1969). The production of He^3 below 20 MeV/nucleon comes from the reaction N^{14} (p, He^3)C^{12} which has a very low threshold energy (4.71 MeV). At 13 MeV the data of MacLeod and Reid (1966) gives a cross section of 28 mb. At lower energies we calculate the cross section from data on the inverse reaction, $C^{12} + He^3 \rightarrow N^{14} + p$ (Kuan, Bonner and Risser 1964) by using the detailed balance principle. After averaging over resonances, some representative values are: σ(7MeV) $\simeq$ 1.9mb, σ(8MeV) $\simeq$ 11mb, σ(10MeV) $\simeq$ 18mb. Above 25 MeV/nucleon the data merges with the cross sections given by Ramaty and Lingenfelter (1969).

Beside the production cross sections, we also need the angular and energy distributions of the secondary products. For the 2-body reaction, $p+\alpha \rightarrow H^2 + He^3$, we use a fit to the angular distributions as given by Ramaty and Lingenfelter (1969). An important feature of this distribution is that in the c.m. (center-of-mass) frame the deuteron is emitted in the forward direction, while the He^3 is coming out in the backward direction. This anisotropy becomes more pronounced with increasing projectile energy.

For the rest of the pα reactions, where there are 3 or more particles in the final state (3-body reactions), the available experimental data is less complete. Ramaty and Lingenfelter (1969) assumed that for these reactions the velocity of the secondary particle in the c.m. frame is always less than or equal to the velocity of the center of mass. As a consequence, in the laboratory frame the secondary particle is always emitted in the forward direction. This can be compared with the data: At an incident energy of 300 MeV the angular distribution of deutrons from 3-body reactions is strongly peaked in the forward direction in the laboratory frame (Innes 1957). At 95 MeV, the He^3 angular distribution is also peaked in the forward direction (Tannenwald 1958), but at 300 MeV, a substantial fraction of the He^3 nuclei are emitted in the backward direction as well (Innes 1957). Thus, the assumption of Ramaty and Lingenfelter (1969) gives correct results regarding the concentration of deuterons in the forward direction, but it underestimates the amount of He^3 produced in the backward direction. There is no data on the angular distribution of tritium, but in analogy to He^3, we expect that the above assumption would also underestimate the amount of tritium emitted in the backward direction.

We perform our calculations for two limiting models: a thick-target model in which the accelerated particles move from the flare region downwards into the Sun, undergoing nuclear interactions as they slow down in the solar atmosphere; and a thin-target model in which the spectrum of accelerated particles is not modified during the time in which the nuclear interactions take place. The latter model assumes that either the total path length traversed by the particles at the

Sun is small in comparison with their interaction length, or that the particle energy loss from ionization and nuclear interactions is just balanced by energy gains from acceleration.

Let us first consider the thick-target model. For this model we assume that the primary particles are collimated into a beam directed downward into the Sun. We define the direction of the beam as the forward direction. Because we can assume that the primary particles are slowed down mainly by ionization losses, the total number of secondary particles per unit energy per nucleon and unit solid angle produced from a particular type of reaction during the slowing down of the primary particle is given by

$$\frac{dN_s(E_s,\mu)}{d\Omega} = \frac{n_t}{n_H}\int_0^\infty dE' N(E') \int_0^{E'} \frac{1}{m_p}\frac{dx}{dE}(E)\,\frac{d^2\sigma(E,E_s^*,\mu^*)}{dE_s^*\,d\Omega^*}\left[\frac{\partial(E_s,\mu)}{\partial(E_s^*,\mu^*)}\right]^{-1} dE. \tag{3}$$

Here (E_s,μ) and (E_s^*,μ^*) are the energies per nucleon and directional cosines of the secondary particle in the frame of the Sun and the c.m. frame, respectively, with $\mu = 1$ and $\mu^* = 1$ corresponding to the forward direction; n_t and n_H are the target nuclei and proton densities in the ambient medium and m_p is the proton mass; $N(E)$ is the initial number of primary particles in the beam per unit energy per nucleon; dE/dx is the stopping power for the primary particles in the solar atmosphere; $d^2\sigma(E,E_s^*,\mu^*)/dE_s^* d\Omega^*$ is the differential cross section in the c.m. frame for producing a secondary particle of energy E_s^* and directional cosine μ^*; and $\partial(E_s,\mu)/\partial(E_s^*,\mu^*)$ is the Jacobian of transformation between (E_s,μ) and (E_s^*,μ^*). This transformation is

$$\gamma_s = \gamma_c\gamma_s^* + (\gamma_c^2-1)^{1/2}\, p_s^*\mu^* \tag{4}$$

$$\mu = ((\gamma_c^2-1)^{1/2}\ \gamma_s^* + \gamma_c p_s^* \mu^*)/p_s, \tag{5}$$

where γ_c is the Lorentz factor of the center of mass in the frame of the Sun, $\gamma_s = 1+E_s/m_p$, $\gamma_s^* = 1+E_s^*/m_p$, and p_s and p_s^* are momenta corresponding to E_s and E_s^*, respectively. The Lorentz factor γ_c, is a unique function of the incident energy E, and is given by

$$\gamma_c = (E_{cm}^{\ 2} + m_t^{\ 2} - m_i^{\ 2})/(2m_t E_{cm}), \tag{6}$$

where E_{cm} is the total available energy in the c.m. frame, and m_i and m_t are the masses of the projectile and target, respectively.

In evaluating equation (3) we distinguish between cases where the final state consists of 2 particles and cases where the final state consists of 3 or more particles. For a 2-particle final state, $E_s^* = E_m^*$; E_m^* is a function of the incident energy E,

$$\gamma_m^* = (E_{cm}^2 + m_s^2 - m_r^{\ 2})/(2m_s E_{cm}) , \tag{7}$$

where $\gamma_m^* = 1 + E_m^*/m_s$, m_s is the mass of the secondary particle under consideration, and m_r is the mass of the other secondary particle. For a 3-particle final state, E_s^* has a range of values up a maximum given by equation (7), where now m_r is the sum of the masses of all the other secondary particles.

In the absence of detailed experimental data on the angular and energy distributions in 3-body reactions, following Ramaty and Lingenfeleter (1969), we make the assumption that E_s^* is a unique function of E. For $p\alpha$ reactions this function is given by, $E_s^* = E_m^*$ for $\gamma_m^* < \gamma_c$ and $E_s^* = m_s(\gamma_c-1)$ otherwise. For αp reactions, for a given E_{cm}, E_s^* is the same as the E_s^* for $p\alpha$ reactions with the same E_{cm}.

If the c.m. energy of the secondary particle is a unique function of the incident energy, E, then the center-of-mass differential cross

section be written as

$$\frac{d^2\sigma(E,E_s^*,\mu^*)}{dE_s^*\, d\Omega^*} = \frac{1}{2\pi}\ \sigma(E)\ P(E,\mu^*)\ \delta(E_s^*-E_m^*). \tag{8}$$

Here $\sigma(E)$ is the total cross section as a function of energy, and $P(E,\mu^*)\ d\mu^*$ is the probability that in the c.m. frame the secondary particle will have directional cosine in $d\mu^*$ around μ^*. By substituting equation (8) into equation (3), and by interchanging the orders of integration, we obtain

$$\frac{dN_s}{d\Omega}(E_s,\mu) = \frac{n_t}{n_H}\frac{\sigma(E)}{m_p}\frac{dx}{dE}\frac{dE}{dE_m^*}\frac{P(E,\mu^*)}{2\pi}\left[\frac{\partial(E_s,\mu)}{\partial(E_s^*,\mu^*)}\right]^{-1} N(>E), \tag{9}$$

where $N(>E)$ is the initial number of primary particles in the beam with energies per nucleon greater than E. All quantities on the r.h.s. of equation (9) are functions of E and μ^*. For a given E_s and μ, E is obtained by solving the equation

$$\gamma_s^* = \gamma_c\gamma_s\ -(\gamma_c^{\,2}-1)^{1/2}\ p_s\mu, \tag{10}$$

where both γ_s^* and γ_c are functions of E; the directional cosine μ^* is then obtained by evaluating the equation

$$\mu^* = (\gamma_c p_s\mu - \gamma_s\ (\gamma_c^2-1)^{1/2})\ /p_s^*. \tag{11}$$

The Jacobian in equation (9) is given by

$$\frac{\partial(E_s,\mu)}{\partial(E_s^*,\mu^*)} = \left[1+\frac{d\gamma_c}{d\gamma_s^*}\frac{p_s^*}{(\gamma_c^2-1)^{1/2}}\mu^*\right]\frac{p_s^*}{p_s}. \tag{12}$$

We have evaluated equation (9) numerically for the various reactions listed in Table 1, and with σ and P as given by the experimental data discussed above. These calculations were carried out for a variety of values for E_s and μ, as well as for various primary spectra. Some of these results will be presented in the discussion below.

If we integrate equation (9) over $d\Omega$ we obtain the total number of secondary particles per unit energy interval

$$N_s(E_s) = 2\pi \int d\mu \, \frac{dN_s(E_s,\mu)}{d\Omega} \tag{13}$$

For a fixed E_s, the transformations of equations (4) and (5) imply that μ is a unique function of E_s^*, which in turn is a unique function of E by our assumptions. We can thus transform the integration variable in equation (13) from μ to E. For the derivative $d\mu/dE$ we find

$$\frac{d\mu}{dE} = \frac{\partial(E_s,\mu)}{\partial(E_s^*,\mu^*)} \, \frac{dE_s^*}{dE} \left[\frac{\partial E_s}{\partial \mu^*}\right]^{-1}. \tag{14}$$

Then, by substituting equations (9) and (14) into equation (13) we obtain

$$N_s(E_s) = (n_t/n_H) \int_0^\infty N(>E) \, \frac{\sigma(E)}{m_p} \, \frac{dx}{dE} \, f(E,E_s) \, dE, \tag{15}$$

where

$$f(E,E_s) = P(E,\mu^*)\left(\frac{\partial E_s}{\partial \mu^*}\right)^{-1} = P(E,\mu^*)(\gamma_c^2-1)^{-1/2} \, (\gamma_s^*-1)^{-1/2} \, m_s^{-1} \tag{16}$$

is the probability that in the laboratory frame the energy of the secondary particle will be in dE_s around E_s. Equation (15) could have been obtained directly from elementary consideration, but we need the full formalism in order to calculate the angular distributions.

For the thin-target model, the equations analogous to equations (3) and (15) are

$$\frac{dN_s}{d\Omega}(E_s,\mu) = \frac{n_t}{n_H} x_1 \int_0^\infty N(E) \, \beta(E) \, \frac{1}{m_p} \, \frac{d^2\sigma(E,E_s,\mu^*)}{dE_s^* \, d\mu^*} \left[\frac{\partial(E_s,\mu)}{\partial(E_s^*,\mu^*}\right]^{-1} dE \tag{17}$$

and

$$N_s(E_s) = \frac{n_t}{n_H} x_1 \int N(E) \, \beta(E) \, \frac{\sigma(E)}{m_p} \, f(E,E_s) dE, \tag{18}$$

where $x_1 = m_p n_H c t_1$ is the total path length traversed by relativistic

primary particles in the interaction time t_1, β is velocity in units of c, and N(E) is the number of primary particles per unit energy per nucleon in the interaction region. For this model, however, we do not need the equivalent to equation (9), because we shall evaluate isotope production in the backward hemisphere for the thick-target model only.

III. Numerical Results

In Figures 1, 2, and 3 we show the H^2, H^3 and He^3 production as evaluated from equation (9) and (13) for the thick-target model. Here the primary particles have exponential rigidity spectra with P_o = 150 MV. The numerals on the various curves correspond to the reactions listed in Table 1 and the total curve is the sum of these partial production modes. Except for the backward spectra, all curves in Figures 1, 2 and 3 represent isotope productions integrated over all directional cosines, $-1 \leq \mu \leq 1$. The backward spectra are obtained by integrating equation (13) over $-1 \leq \mu \leq 0$ only.

We first consider the spectra integrated over all angles. We see that isotope production below about 10 MeV/nucleon is due entirely to $p\alpha$ reactions. This is a model independent result, as can be seen from Table 1. Here, the minimum energies of secondary particles, E_s (min), for αp reactions are about 10 MeV/nucleon and therefore these reactions cannot contribute to isotope production at lower energies.

Above about 20 MeV/nucleon αp reactions make a major contribution to the total H^3 and He^3 production. For deuterium the $p\alpha$ reactions remain important in this energy region as well. Moreover, around 100 MeV/nucleon most of the H^2 comes from the reaction $p+p \rightarrow d+\pi^+$ It should be noted, however, that the relative contribution of the αp reactions depends on the assumed ratio of the flare-accelerated alpha particles to protons; it is known that this ratio can be energy dependent and time variable. It is important to realize however, that the calculated spectra

below about 10 MeV/nucleon are independent of this variability.

We now consider the backward spectra. Because of our assumptions on the c.m. energy distributions, we obtain secondary particles in the backward direction only from reactions (1) and (10). For deuterium, this result is consistent with the experimental data discussed above, but for H^3 and He^3 we might expect a contribution to the backward spectra also from the 3-body reactions. The forward peaking of the H^2 in the 2-body reactions is also responsible for the relatively low contribution of reaction (1) to the total H^2 production at low energies and its relatively high contribution at larger energies.

In Figures 4 and 5 we present $\Gamma(He^3/H^2)$, the ratio of the backward He^3 to H^2 at the same energy per nucleon. These results are for the thick-target model, with exponential and power-law spectra, respectively. From the above discussion, these ratios are lower limits, because of the additional backward contributions to He^3 from 3-body reactions. If we assume that Innes' (1957) data at 300 MeV is representative, then about 1/3 of the total He^3 in 3-body reactions is emitted in the backward direction. Then from Figure 3 we estimate that the backward He^3/H^2 ratios in Figures 4 and 5 could be larger by factors of 2 to 3. Another source of uncertainty in these ratios is caused by poor cross sectional data for the reaction $p+\alpha \rightarrow H^2+He^3$ above $\sim$ 400 MeV. Because we have assumed that in this energy region the cross section is zero (Meyer 1972), any finite value for it will further increase the He^3/H^2 ratios in Figures 4 and 5. This increase, however, should be small, because we do not expect many flare accelerated protons at high energies.

In Figures 6, 7 and 8 we show the total H^2, H^3 and He^3 production for the thin-target model for various spectra of the primary particles. These figures have been obtained from equation (18), with N(E) given either by equation (2) with P_o = 50MV and 300 MV, or by equation (1) with s = 2 and 4, and for x_1 = 1 gcm^{-2}. As can be seen, below about 10 MeV/nucleon the secondary spectra are only weakly dependent on the spectra of the primary particles. This results from the fact that these secondary nuclei are produced mainly by 3-body pα reactions. From the experimental data (e.g. Ramaty and Lingenfelter 1969) it follows that in these reactions the energy spectra of the secondary particles are independent of the projectile energy. At higher energies, however, the secondary specta tend to resemble the spectra of the primary particles.

IV. Comparison with Observational Data

We start the comparison of our calculations with observational data for the August 1972 events for which both accelerated He^3 and nuclear gamma rays were observed. According to Webber et al. (1974) $\Gamma(He^3/He^4)$, the He^3/He^4 ratio at the same energy per nucleon, is about 0.02 at 60 MeV/nucleon, and it decreases monotonically with decreasing energy to about 0.002 at $\sim$ 7 MeV/nucleon.

Using our calculations as presented in Figure 8 (together with additional unplotted calculations), we plot in Figure 9 $\Gamma(He^3/He^4)$ for the thin-target model with power law primary spectra characterized by various values of s. At $\sim$ 60 MeV/nucleon, $\Gamma(He^3/He^4) \simeq 0.01\ x_1$. By comparing this with the observed ratio, we get that $x_1 \simeq 2\ gcm^{-2}$, and $x(60\ MeV/nucleon) = \beta\ x_1 \simeq 0.7\ gcm^{-2}$. Because the stopping range of a 60 MeV/nucleon He^3 in hydrogen is about 1 gcm^{-2} (Barkas and Berger 1964), the He^3 nuclei will escape from the production region without much attenuation.

Let us compare this result with the gamma-ray observations. According to Chupp et al. (1973), the average flux in the 2.2 MeV line, over a time interval which coincides approximately with the flash phase of August 4, 1972 flare (0623 to 0633 U.T.), was about 0.3 photons $cm^{-2}s^{-1}$. The 2.2 MeV line is due to neutron capture on hydrogen, the neutrons being produced by nuclear interactions of accelerated changed particles (e.g. Ramaty and Lingenfelter 1973). We can estimate the average number of protons in the flare region as follows: From the calculations of Wang and Ramaty (1974), the efficiency of gamma-ray production by neutron capture on hydrogen in the solar atmosphere is about 0.1. The observed 2.2 MeV flux then implies an

average rate of neutron production of $\sim 10^{28}$ neutrons s^{-1}. Using available calculations of neutron production (e.g. Ramaty, Cline and Fisk 1972), this rate then gives that $n_H N_p(>30\text{MeV}) \simeq 1.5 \times 10^{44} \text{cm}^{-3}$, where $N_p(>30\text{MeV})$ is the average number of protons present in the flare region during the gamma-ray observations. We note that, whereas the isotope data determines the product of the ambient density and the interaction time, ($n_H t_1 \simeq 4 \times 10^{13} \text{cm}^{-3}\text{s}$), the gamma-ray data gives the product of the same ambient density and the average number of protons in the interaction region. If we combine these 2 products, we get for the August 4, 1972 flare

$$N_p(>30\text{MeV})/t_1 \simeq 4 \times 10^{30} \text{ protons } s^{-1}. \qquad (19)$$

The quantity given by equation (19) in the rate of proton release from the flare region. The total number of protons released is the product of this rate and the acceleration time, T. For the August 4, 1972 flare T is $\sim 10^3$ seconds as indicated by the microwave data (Toyokawa Observatory, private communication, 1972). The total number of protons released above 30MeV is therefore about 4×10^{33}.

This number should be compared with the total number of protons in the interplanetary medium as deduced from charged particle observations. From the estimates of Ramaty and Lingenfelter (1973) this quantity is about 2×10^{34} protons with energies greater than 30 MeV. The discrepancy of about an order of magnitude between this result and that obtained above from the nuclear reactions is probably due to uncertainties in the measurement of the extremely large particle flux in the interplanetary medium and the estimate of the volume that contains these

particles. We note that the number 2×10^{34} is based on the measurements of Kohl, Bostrom and Williams (1973). Because the proton flux given by these authors could have been too large by at least a factor of 3 (M. Van Hollebeke, private communication 1972), the above discrepancy could be reduced by at least this factor.

In addition to the August 1972 events, H and He isotopes were detected also from other solar flares (Schaeffer and Zahringer 1962; Hsieh and Simpson 1970; Dietrich 1973; Anglin, Dietrich and Simpson 1973a; Garrard, Stone and Vogt 1973). There are no reported observations of H^2 and H^3 from individual flares; Anglin, Dietrich and Simpson (1973a) only present H^2/H^1 and H^3/H^1 ratios, averaged over several solar flares. At $\sim$ 10MeV/nucleon, $\Gamma(H^2/H^1) \simeq 8 \times 10^{-5}$ and $\Gamma(H^3/H^1) \simeq 2 \times 10^{-5}$. Using our calculations as presented in Figures 6 and 7 (together with additional unplotted calculations), we give in Figures 10 and 11 $\Gamma(H^2/H^1)$ and $\Gamma(H^3/H^1)$ for the thin-target model with power law primary spectra characterized by various values of δ. For $2 \leq s \leq 3$, the observation $\Gamma(H^2/H^1) \simeq 8 \times 10^{-5}$ at 10 MeV/nucleon implies that x_1 is between .5 to 1.5 gcm^{-2}, and that x(10 MeV/nucleon) = βx_1 is between 0.08 to 0.2 gcm^{-2}. These path lengths are consistent with the H^3 observations, as can be seen by using the results of Figure 11. They are also quite comparable with the path length deduced from the He^3/He^4 ratio of the August 1972 events. We note that because the stopping ranges of 10 MeV/nucleon H^2 and H^3 in hydrogen are about 0.1 gcm^{-2} and 0.15 gcm^{-2}, these nuclei can escape from the production region without much attenuation.

However, the average He^3/He^4 ratio of about 2×10^{-2} at ~ 10 MeV/nucleon used by Anglin, Dietrich and Simpson (1973a) to compare with their H^2/H^1 ratios is inconsistent with these values of x_1. Indeed as can be seen from Figure 9, $\Gamma(He^3/He^4) \simeq 2 \times 10^{-2}$ requires an x_1 ranging from about 20 gcm^{-2} to 60 gcm^{-2} for $2 \leq s \leq 3$. This could indicate that the average He^3/He^4 ratios are greatly modified by a subset of flares which are enriched in He^3.

There are observations of He^3-rich events. Thus, $\Gamma(He^3/He^4)$ for the flare of October 14, 1969 was about 0.3 from a few MeV/nucleon to about 20 MeV/nucleon (Garrard, Stone and Vogt 1973, Anglin 1974). Furthermore, for the flare of July 30, 1970 the He^3/He^4 ratio was about 0.5 from about 10 to 20 MeV/nucleon (Anglin 1974). A common feature of these He^3 rich events is absence of H^2 and H^3. The lower limits on $\Gamma(He^3/H^2)$ and $\Gamma(He^3/H^3)$ are, in some cases, as large as 20.

We wish to suggest that in these He^3-rich events we observe predominantly the products of nuclear interactions in the backward hemisphere w.r.t. the direction of the primary beam. A plausible model is one where the primary beam is directed downwards into the Sun, as in the thick-target model discussed above.

As can be seen from Figures 4 and 5, $\Gamma(He^3/H^2)$ for the backward hemisphere can become as large as observed for He^3-rich events. However, because this calculated enrichment occurs mainly at the very low energies ($\lesssim$10 MeV/nucleon), the isotopes have to be accelerated after their production. The need for post-production acceleration also follows from the fact that the He^3 nuclei at the observed energies have much

shorter stopping ranges than the path length required for their production (Anglin, Dietrich and Simpson 1973b). Alternatively, in the thick-target model, the He^3 nuclei emitted in the backward direction probably have to go through a path length equal to the stopping range of the primary downward moving protons. Because these He^3 nuclei are produced by protons in the range 50 to 200 MeV, this path length is about 1 to 10 gcm^{-2}. Since this range of values is much larger than the stopping length of the low energy He^3 nuclei, post production acceleration is again required.

There is no data on the laboratory angular distribution of H^3. According to our kinematical assumption (Section II), the tritium should be emitted in the forward direction; hence, as deuterium, it should not be observable in He^3-rich events. However, even if some H^3 is emitted in the backward direction, it will be destroyed in nuclear reactions.

Figure 12 shows the destruction cross sections of H^2, H^3 and He^3. Cross sections for the reaction $H^3(p,n)He^3$ are from Hanson, Taschek and Williams (1949) and from Goldberg et al. (1961); cross sections for the reactions $p+H^2 \rightarrow 2p+n$ and $p+He^3 \rightarrow d+2p$ are from Meyer (1972); and cross sections for the reaction $He^3(\alpha,p)Li^6$ are obtained by using the detailed balance principle and data on the inverse reaction $Li^6(p,\alpha)He^3$ (Yeronymo, Mani, and Sadeghi 1963; Marion, Weber and Mozer 1956; Hub, Clement and Wildermuth 1972). As can be seen, H^3 has the largest destruction cross section at low energies; moreover, H^3 is transformed into He^3. The destruction path length of H^3 is about 5 gcm^{-2}, comparable to the range

traversed by the isotopes during post-production acceleration. We expect, therefore, that a large fraction of the backward moving tritium is transformed into He^3. At low energies, He^3 can be destroyed only by alpha particles, but the weighted cross section is small.

Finally, let us estimate the flux in the 2.2 MeV line that is expected from a He^3-rich flare. Because both He^3 nuclei and neutrons are produced primarily in $p\alpha$ reactions (for primary spectra of the type observed from solar flares), we expect the production of about 1 neutron per He^3 nucleus. The efficiency of photon production is about 0.1 (Wang and Ramaty 1974). About 30% of the He^3 is emitted in the backward direction (Section II). Furthermore, the escape probability of charged isotopes should be less than unity even if there is post-production acceleration. Therefore, we define a quantity f, the number of 2.2 MeV photons per escaping He^3 nucleus, and allow it to be a free parameter of order unity. The time-integrated flux of 2.2 MeV photons at earth is therefore

$$\phi(2.2\ \text{MeV}) = (4\pi R^2)^{-1}\ N(He^3)\ f\ \left(\frac{\text{photons}}{\text{cm}^2}\right), \qquad (20)$$

where $N(He^3)$ is the total number of He^3 nuclei released by the flare into the interplanetary medium. We estimate $N(He^3)$ as follows: For both He^3-rich events, October 14, 1969 and July 30, 1970, the alpha particle fluxes at about 10 MeV/nucleon were $\sim 2 \times 10^{-3}$ particles $cm^{-2}s^{-1}sr^{-1}$ $(MeV/nucleon)^{-1}$ (M. Van Hollebeke, private communication). Using a He^3/He^4 ratio of about 0.3, we get that the He^3 flux at this energy is $\sim 6 \times 10^{-4}$. Then using the He^3 spectrum as given by Anglin (1974), we

get a total He^3 intensity of $\sim 10^{-2}$ He^3 $cm^{-2}s^{-1}sr^{-1}$. This He^3 flux is spread over some volume in the interplanetary medium. Ramaty and Lingenfelter (1973) have estimated this volume for the August 1972 events as $\sim 10^{39}cm^3$. Because the He^3- rich events are very much smaller, we take the volume, somewhat arbitrarily, to be $\sim 5 \times 10^{37}cm^3$. Therefore, the predicted 2.2 MeV gamma-ray flux is

$$\phi(2.2 \text{ MeV}) \simeq 3 \text{ f } N(He^3)/10^{28} \quad (\frac{\text{photons}}{cm^2}). \tag{21}$$

This flux should be compared with the observed 2.2 MeV flux from the August 4, 1972 flare which was about 200 photons cm^{-2}. We hope that with improved instrumentation, nuclear gamma rays will be observed from He^3-rich flares.

Acknowledgement

We wish to acknowledge J. D. Anglin, M. Van Hollebeke, F. B. McDonald and B. Teegarden for allowing us to use their data prior to publication.

References

Anglin, J. D. 1974, Invited paper, American Physical Society Meeting Chicago, February 1974.

Anglin, J. D., Dietrich, W. F., and Simpson, J. A. 1973a, Ap. J. (Letters), 186, L4.

Anglin, J. D., Dietrich, W. F., and Simpson, J. A. 1973b High-Energy Phenomena on the Sun, Symposium Proceedings, Edited by R. Ramaty and R. G. Stone (NASA SP-342), p. 315.

Barkas, W. H., and Berger, M. J. 1964, Tables of Energy Losses and Ranges of Heavy Charged Particles, NASA SP-3073.

Cameron, A. G. W. 1973, Space Sci. Rev. 15, 121.

Chupp, E. L., Forrest, D. J., Higbie, P. R., Suri, A. N., Tsai, C., and Dunphy, P. P. 1973, Nature, 241, 333.

Dietrich, W. F. 1973, Ap. J., 180, 955.

Garrard, T. L., Stone, E. C., and Vogt, R. E. 1973, High Energy Phenomena on the Sun, Symposium Proceedings, edited by R. Ramaty and R. G. Stone (NASA SP-342), p. 341

Goldberg, M. D., Anderson, J. D., Stoering, J. P. and Wong, C. 1961, Phys. Rev. 122, 1510.

Hanson, A. O., Taschek, R. F., and Williams, J. H. 1949, Rev. Mod. Phys. 21, 635.

Hsieh, K. C., and Simpson, J. A. 1970, Ap. J. (Letters), 162, 191.

Hub, R., Clement, D., Wildermuth, K. 1972, Z. Physik 252, 324.

Innes, W. H., 1957, U. C. R. L. Rept. No. 8040, University of California Radiation Lab., Berkeley.

Kohl, J. W., Bostrom, C. O., and Williams, D. J. 1973, World Data Center Rept. UAG (part 2), Collected Data Reports on August 1972 Solar

Terrestrial Events.

Kuan, H. M., Bonner, T. W., Risser, J. R. 1964, Nuclear Physics, 51, 481.

Lingenfelter, R. E., and Ramaty, R. 1967, High Energy Nuclear Reactions in Astrophysics, Edited by B. S. P. Shen (W. A. Benjamin, New York), p. 99.

MacLeod, A. M. and Reid, J. M. 1966, Proc. Phys. Soc. 87, 437.

Marion, J. B., Weber, G., and Mozer, F. S. 1956, Phys. Rev. 104, 1402.

Meyer, J. P. 1971, Isotopic Composition of the Primary Cosmic Radiation, Edited by P. M. Dauber, (Danish Space Research Institute, Lyngby, Denmark), p. 235.

Meyer, J. P. 1972, Astron. Astrophys. Suppl. 7, 417.

Ramaty, R. and Lingenfelter, R. E. 1969, Ap. J. 155, 587.

Ramaty, R. and Lingenfelter, R. E. 1973, High Energy Phenomena on the Sun, Edited by R. Ramaty and R. G. Stone (NASA SP-342), p. 301.

Ramaty, R., Cline, T. L., and Fisk, L. A. 1972, Phys. Rev. Letters, 29, 1039.

Schaeffer, O. A., and Zahringer, J. 1962, Phys. Rev. Letters, 8, 389.

Tannenwald, P. O. 1953, Phys. Rev., 89, 508.

Wang, H. T. and Ramaty, R. 1974, Solar Physics, in press.

Webber, W. R., Roelof, E. C., McDonald, F. B., Teegarden, B. J. and Trainor, J. 1974 (preprint).

Yeronymo, J. M. F., Mani, G. S., and Sadeghi, A. 1963, Nuclear Physics, 43, 424.

Table 1

Isotope Production in pp, pα and αp Reactions

Deuterium Production	E_{th} (MeV/nucleon)	E_s (min) (MeV/nucleon)
1. $p + \alpha \rightarrow H^2 + He^3$	23	
2. $\alpha + p \rightarrow H^2 + He^3$	23	9.1
3. $p + \alpha \rightarrow H^2 + p+n$	31.7	
4. $\alpha + p \rightarrow H^2 + p+n$	31.7	12.5
5. $p + \alpha \rightarrow 2H^2 + p$	29.9	
6. $\alpha + p \rightarrow 2H^2 + p$	29.9	11.8
7. $p + p \rightarrow H^2 + \pi^+$	286.5	63.9
Tritium Production		
8. $p + \alpha \rightarrow H^3 + 2p$	24.8	
9. $\alpha + p \rightarrow H^3 + 2p$	24.8	13.1
Helium-3 Production		
10. $p + \alpha \rightarrow He^3 + H^2$	23	
11. $\alpha + p \rightarrow He^3 + H^2$	23	12.2
12. $p + \alpha \rightarrow He^3 + n + p$	24.8	
13. $\alpha + p \rightarrow He^3 + n + p$	24.8	13.1

Figure Captions

1. Deuteron production in the thick-target model for exponential proton and alpha particle spectra with P_o = 150 MV and normalized to 1 proton of energy greater than 30 MeV. The numerals correspond to the reactions of Table 1, and backward indicates production into the entire backward hemisphere.
2. Triton production in the thick-target model for exponential proton and alpha particle spectra with P_o = 150 MV and normalized to 1 proton of energy greater than 30 MeV. The numerals correspond to the reactions of Table 1.
3. Helium-3 production in the thick-target model for exponential proton and alpha particle spectra with P_o = 150 MV and normalized to 1 proton of energy greater than 30 MeV. The numerals correspond to the reactions of Table 1, and backward indicates production into the entire backward hemisphere.
4. The He^3-to-H^2 ratio at the same kinetic energy per nucleon in the backward hemisphere calculated in the thick-target model with exponential spectra with various values of P_o.
5. The He^3-to-H^2 ratio at the same kinetic energy per nucleon in the backward hemisphere calculated in the thick-target model with power law spectra with various spectral indexes.
6. Total deuterium production in the thin-target model for various primary spectra normalized to 1 proton of energy greater than 30 MeV. X_1 is the amount of matter traversed by relativistic particles.

7. Total tritium production in the thin-target model for various primary spectra normalized to 1 proton of energy greater than 30 MeV. X_1 is the amount of matter traversed by relavistic particles.

8. Total helium-3 production in the thin-target model for various primary spectra normalized to 1 proton of energy greater than 30 MeV. X_1 is the amount of matter traversed by relativistic particles.

9. The He^3-to-He^4 ratio at the same kinetic energy per nucleon in the thin-target model for various spectral indexes s.

10. The H^2-to-H^1 ratio at the same kinetic energy per nucleon in the thin-target model for various spectral indexes s.

11. The H^3-to-H^1 ratio at the same kinetic energy per nucleon in the thin-target model for various spectral indexes s.

12. H^2, H^3 and He^3 destruction cross sections.

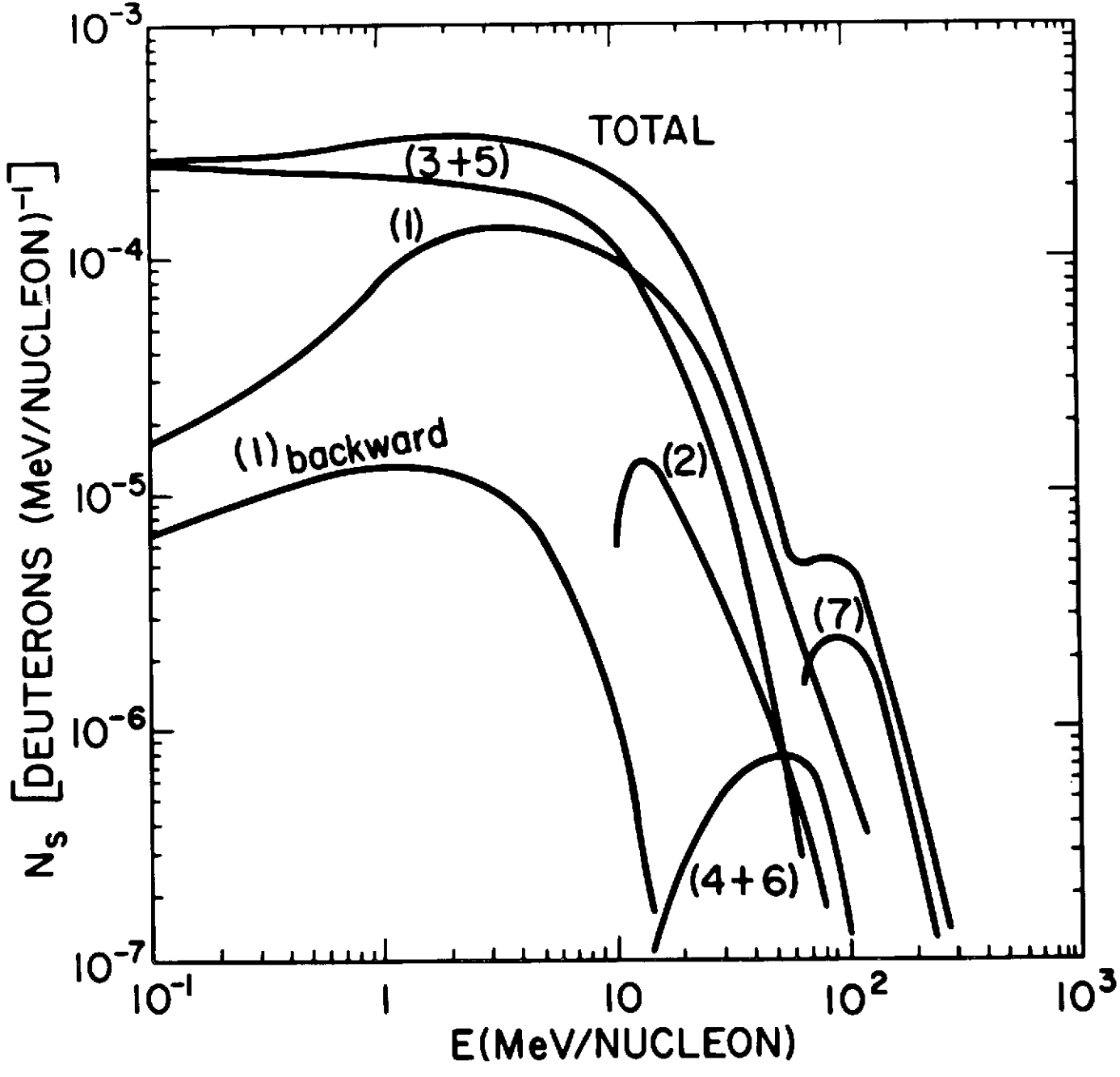
TOTAL
(3+5)
(1)
(1) backward
(2)
(7)
(4+6)
N_s [DEUTERONS (MeV/NUCLEON)$^{-1}$]
E(MeV/NUCLEON)
10^{-3}
10^{-4}
10^{-5}
10^{-6}
10^{-7}
10^{-1}
1
10
10^2
10^3

Figure 1

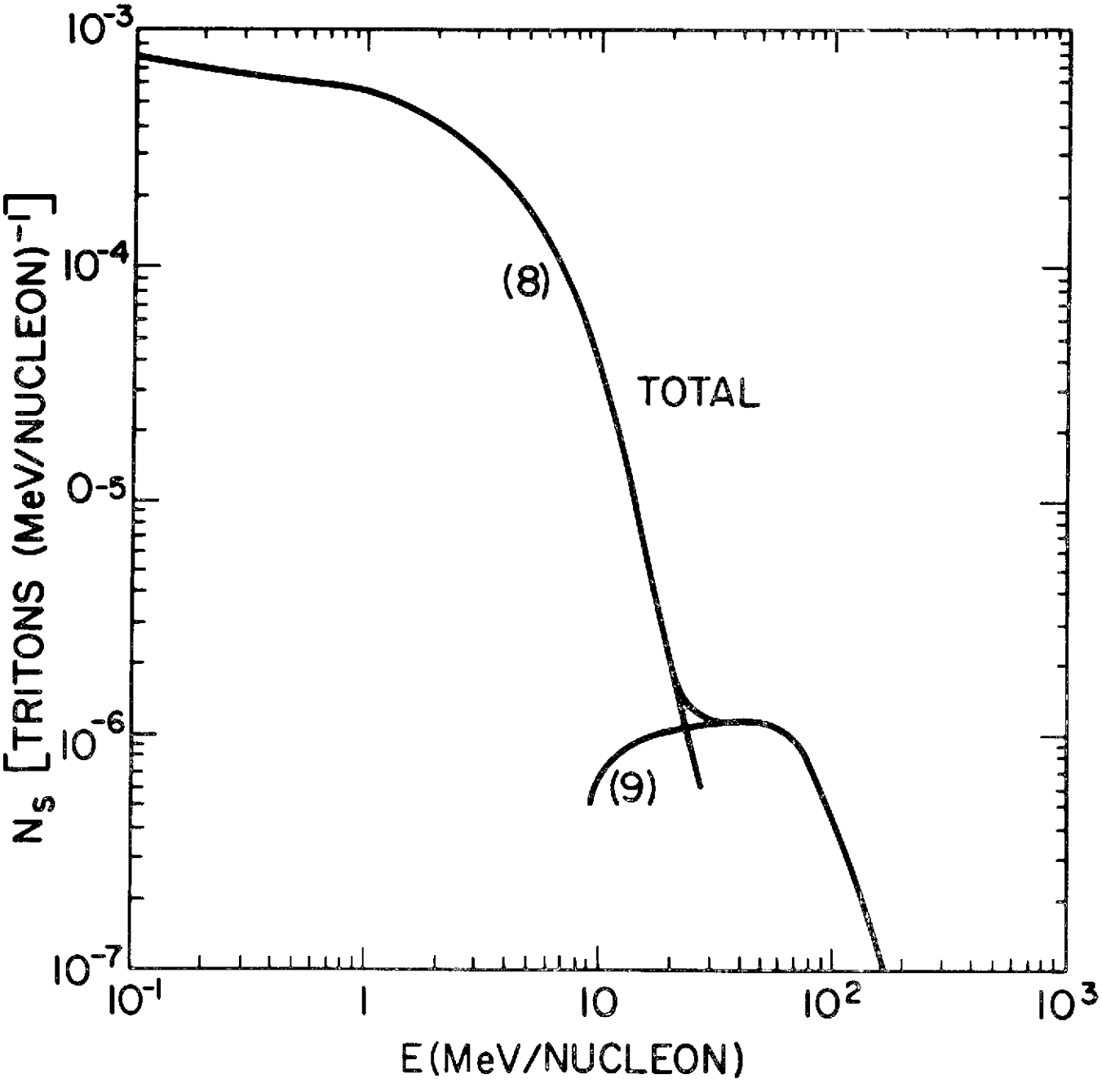
10^{-3}
10^{-4}
0^{-5}
10^{-6}
10^{-7}
N_s [TRITONS (MeV/NUCLEON)$^{-1}$]
(8)
TOTAL
(9)
10^{-1}
1
10
10^2
10^3
E(MeV/NUCLEON)

Figure 2

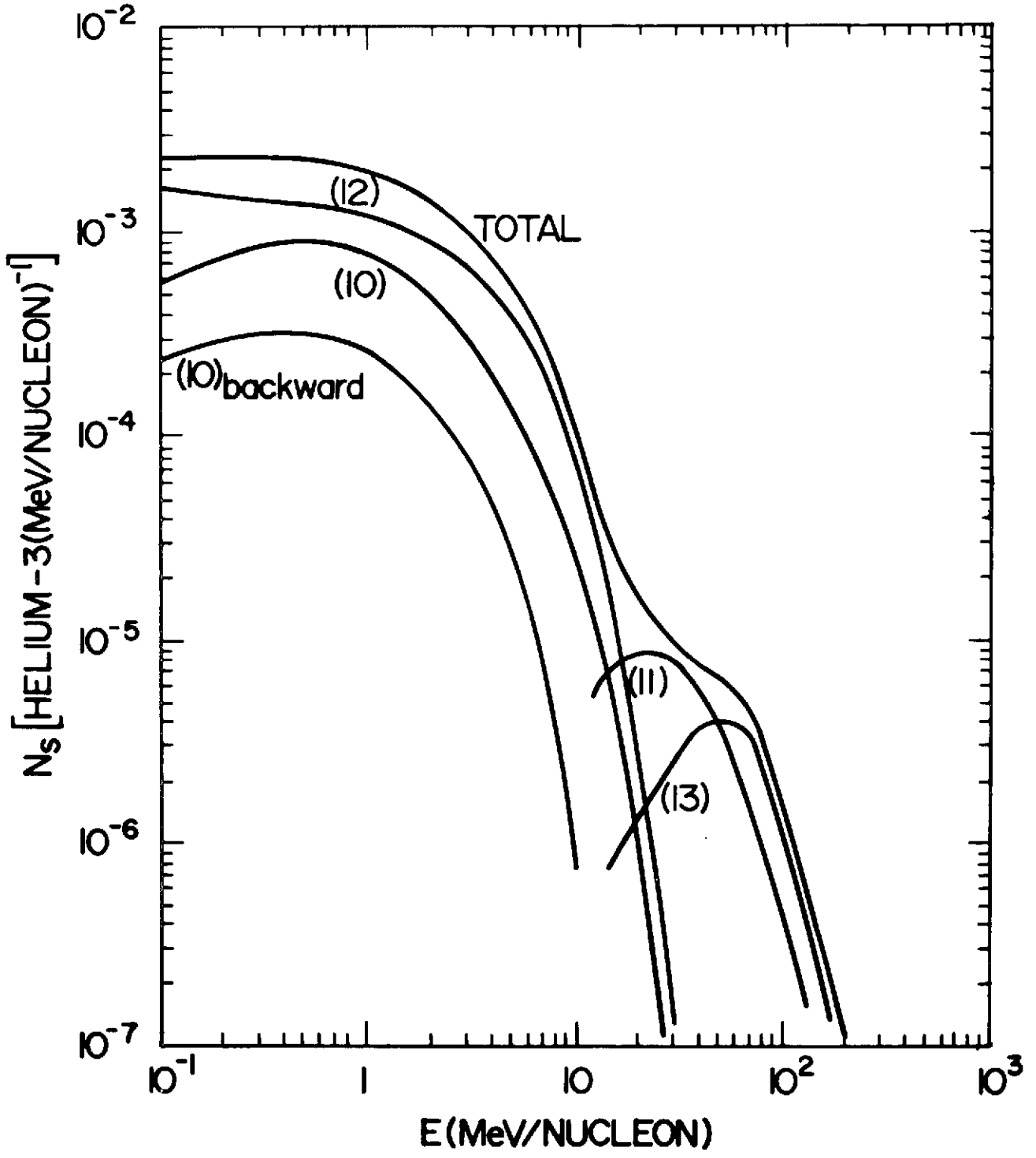
10^{-2}
10^{-3}
10^{-4}
10^{-5}
10^{-6}
10^{-7}
N_S [HELIUM-3(MeV/NUCLEON)$^{-1}$]
(12)
TOTAL
(10)
(10)backward
(11)
(13)
10^{-1}
1
10
10^{2}
10^{3}
E(MeV/NUCLEON)

Figure 3

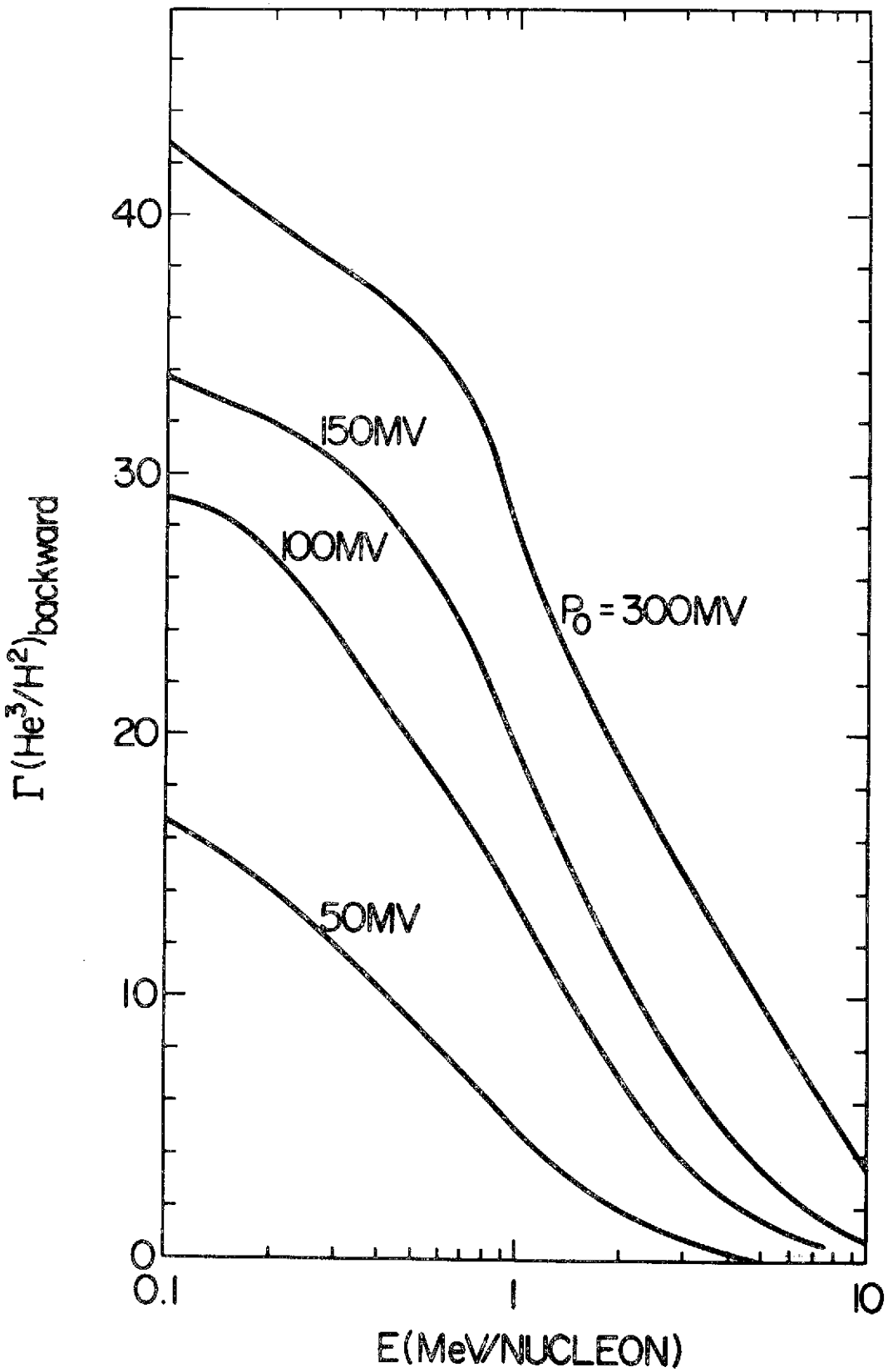
40
30
20
10
0
0.1
1
10
150MV
100MV
50MV
P_0 = 300MV
$\Gamma(He^3/H^2)_{backward}$
E(MeV/NUCLEON)

Figure 4

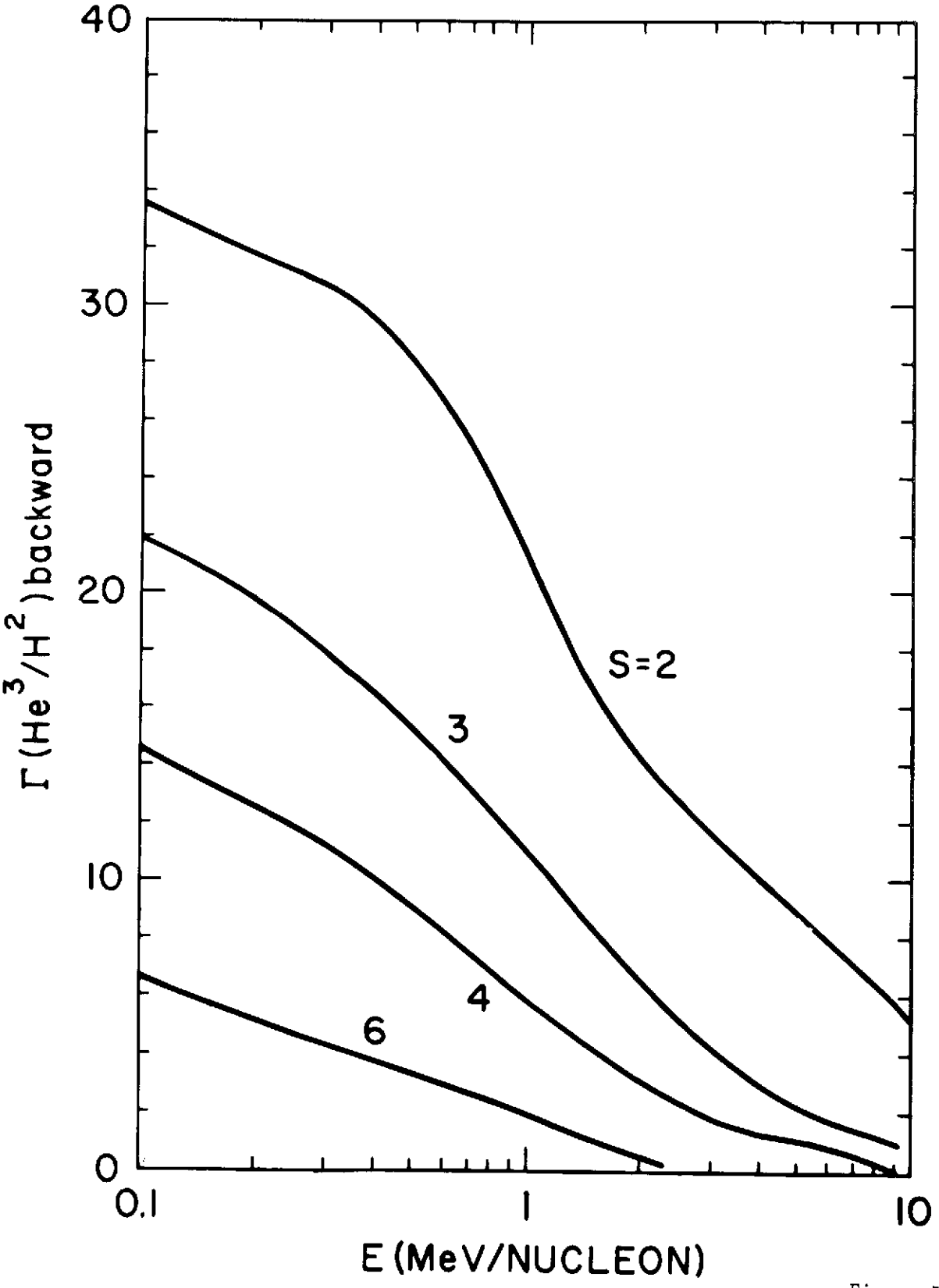

Figure 5

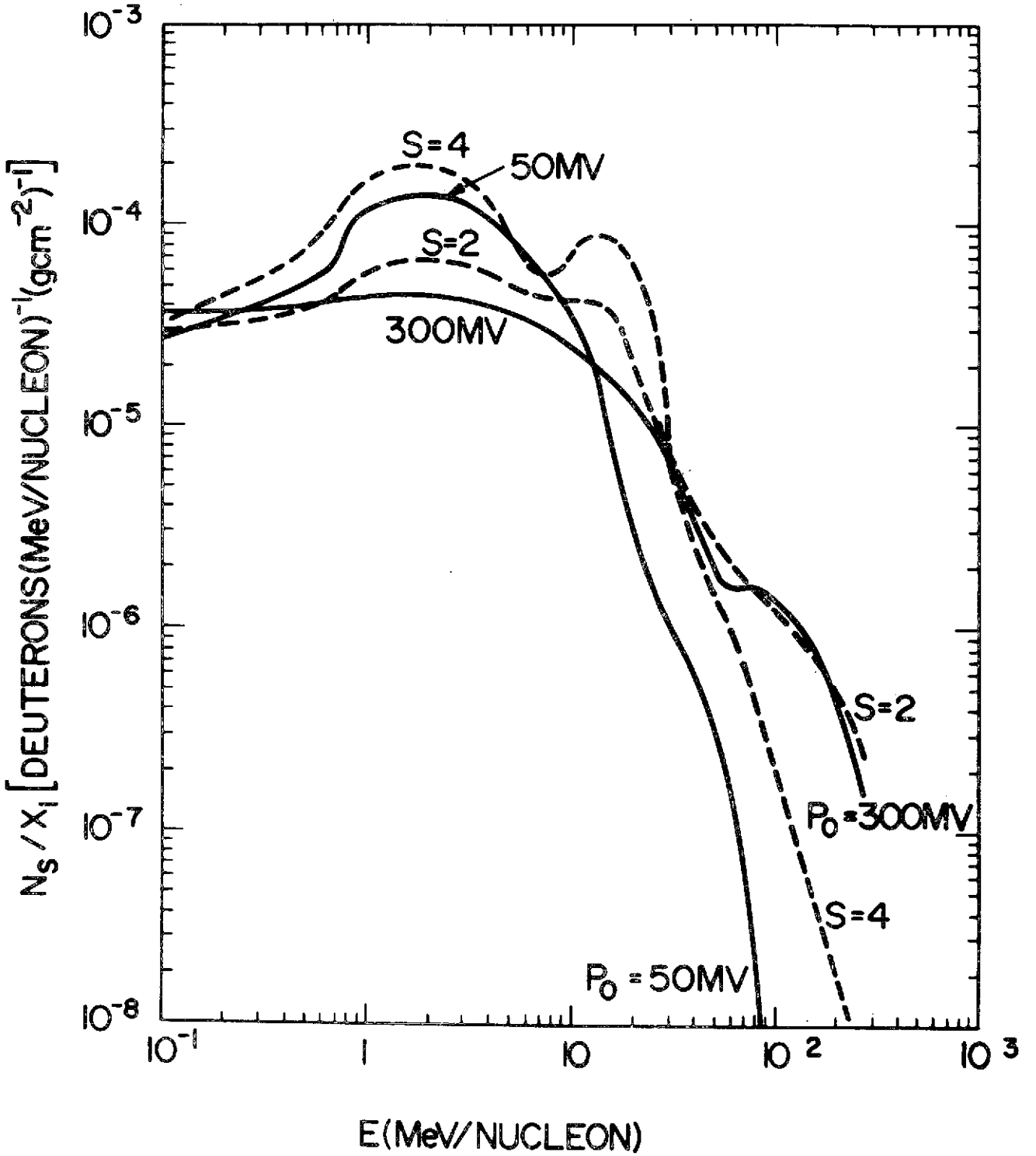
10^{-3}
10^{-4}
10^{-5}
10^{-6}
10^{-7}
10^{-8}
N_S / X_1 [DEUTERONS(MeV/NUCLEON)$^{-1}$(gcm^{-2})$^{-1}$]
S=4
50MV
S=2
300MV
S=2
P_0=300MV
S=4
P_0 = 50MV
10^{-1}
1
10
10^2
10^3
E(MeV/NUCLEON)

Figure 6

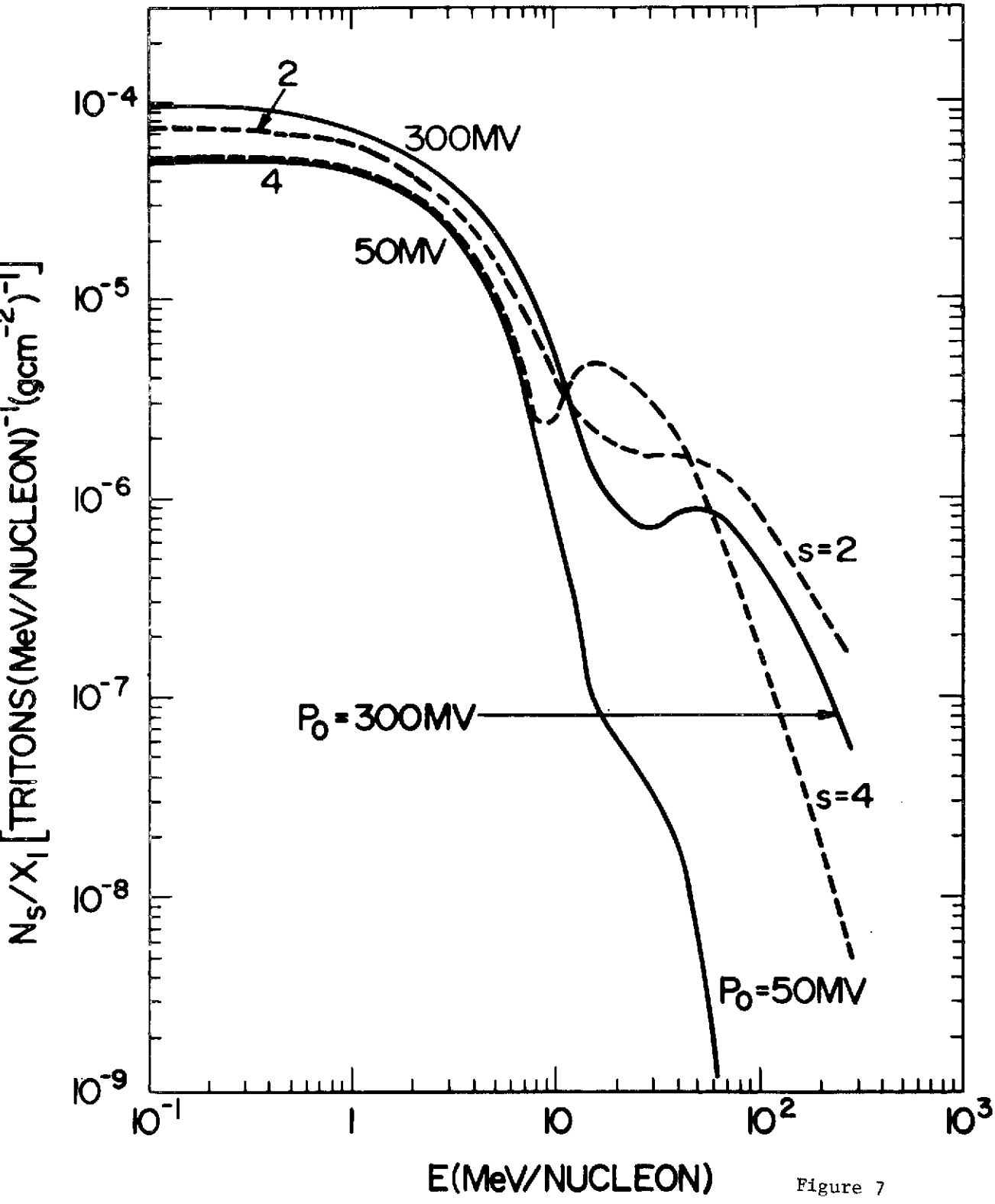
2
4
300MV
50MV
s=2
s=4
P_0 = 300MV
P_0 = 50MV
10^{-4}
10^{-5}
10^{-6}
10^{-7}
10^{-8}
10^{-9}
10^{-1}
1
10
10^2
10^3
N_s/X_1 [TRITONS(MeV/NUCLEON)$^{-1}$(gcm^{-2})$^{-1}$]
E(MeV/NUCLEON)

Figure 7

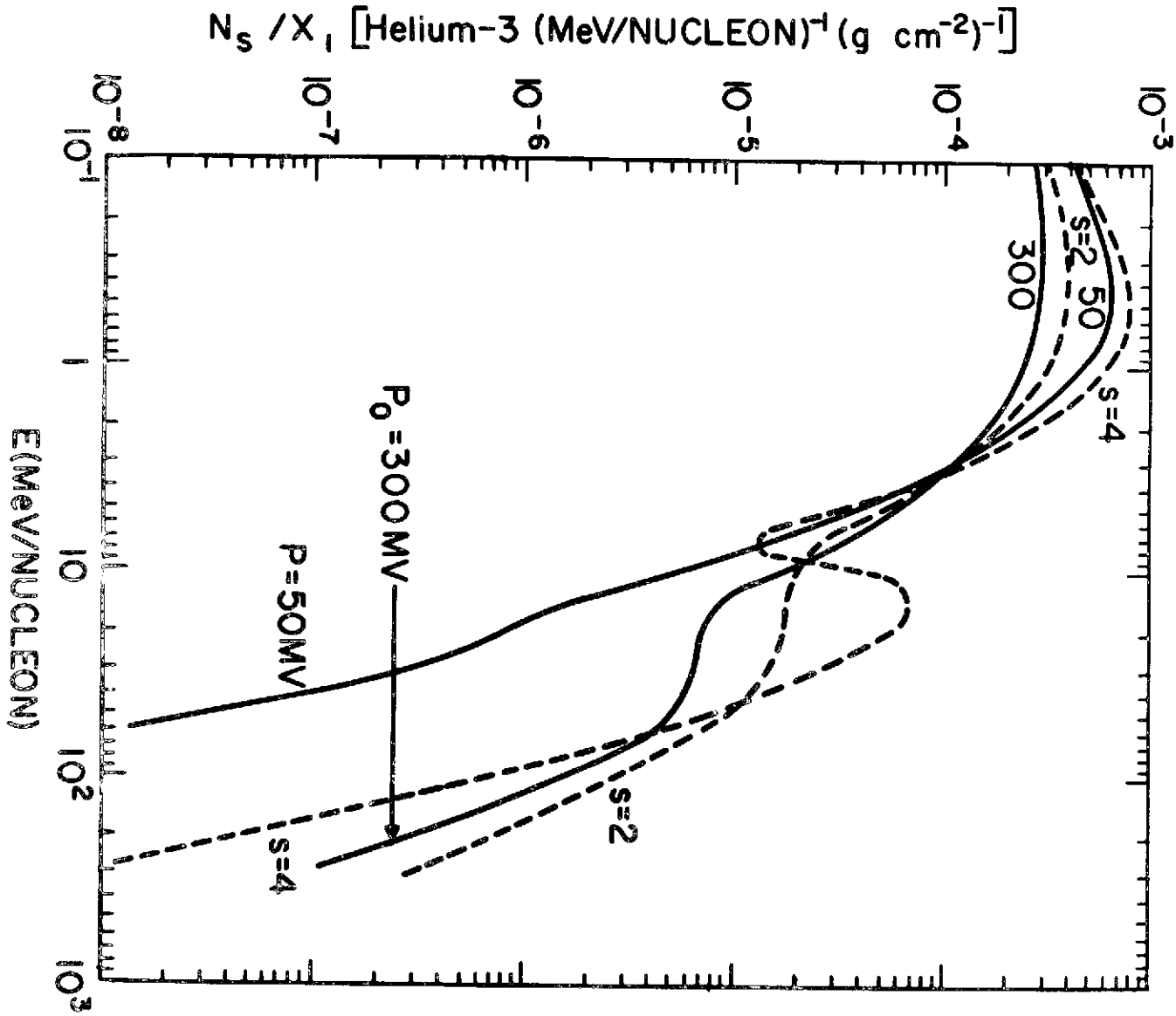
N_S / X_1 [Helium-3 (MeV/NUCLEON)$^{-1}$ (g cm^{-2})$^{-1}$]
10^{-8}
10^{-7}
10^{-6}
10^{-5}
10^{-4}
10^{-3}
10^{-1}
1
10
10^2
10^3
E(MeV/NUCLEON)
300
s=2
50
s=4
P_0=300MV
P=50MV
s=2
s=4

Figure 8

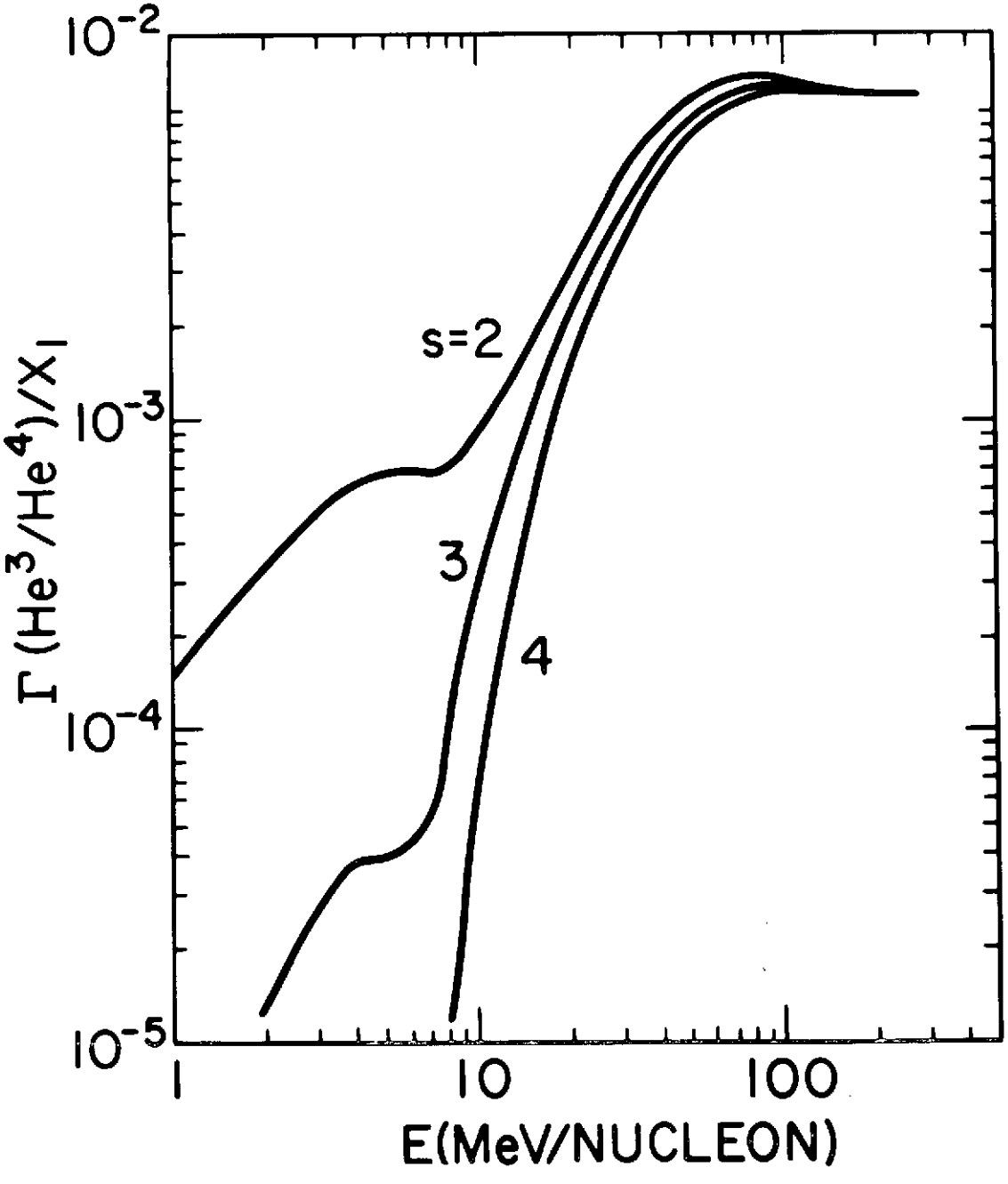

Figure 9

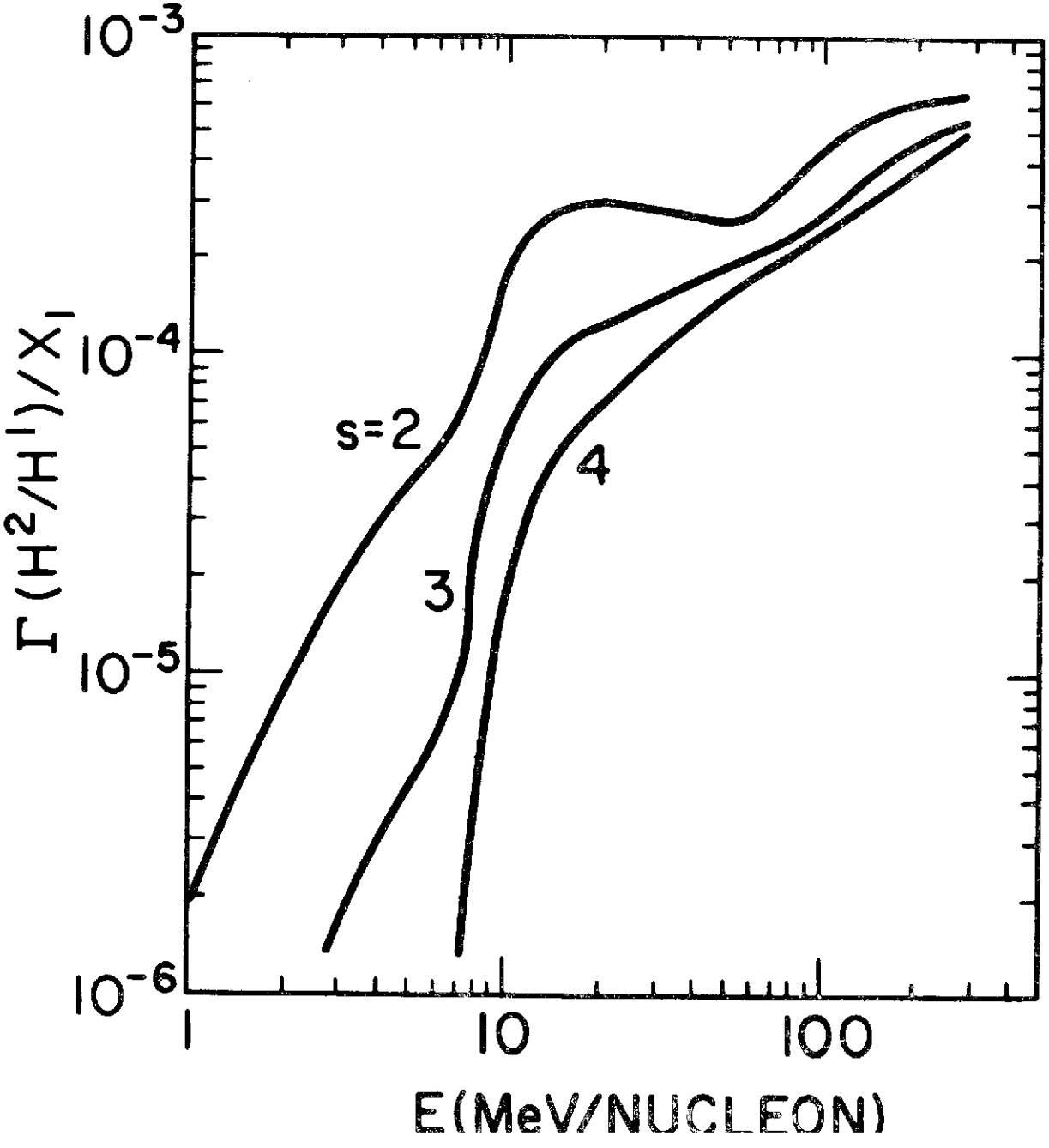

Figure 10

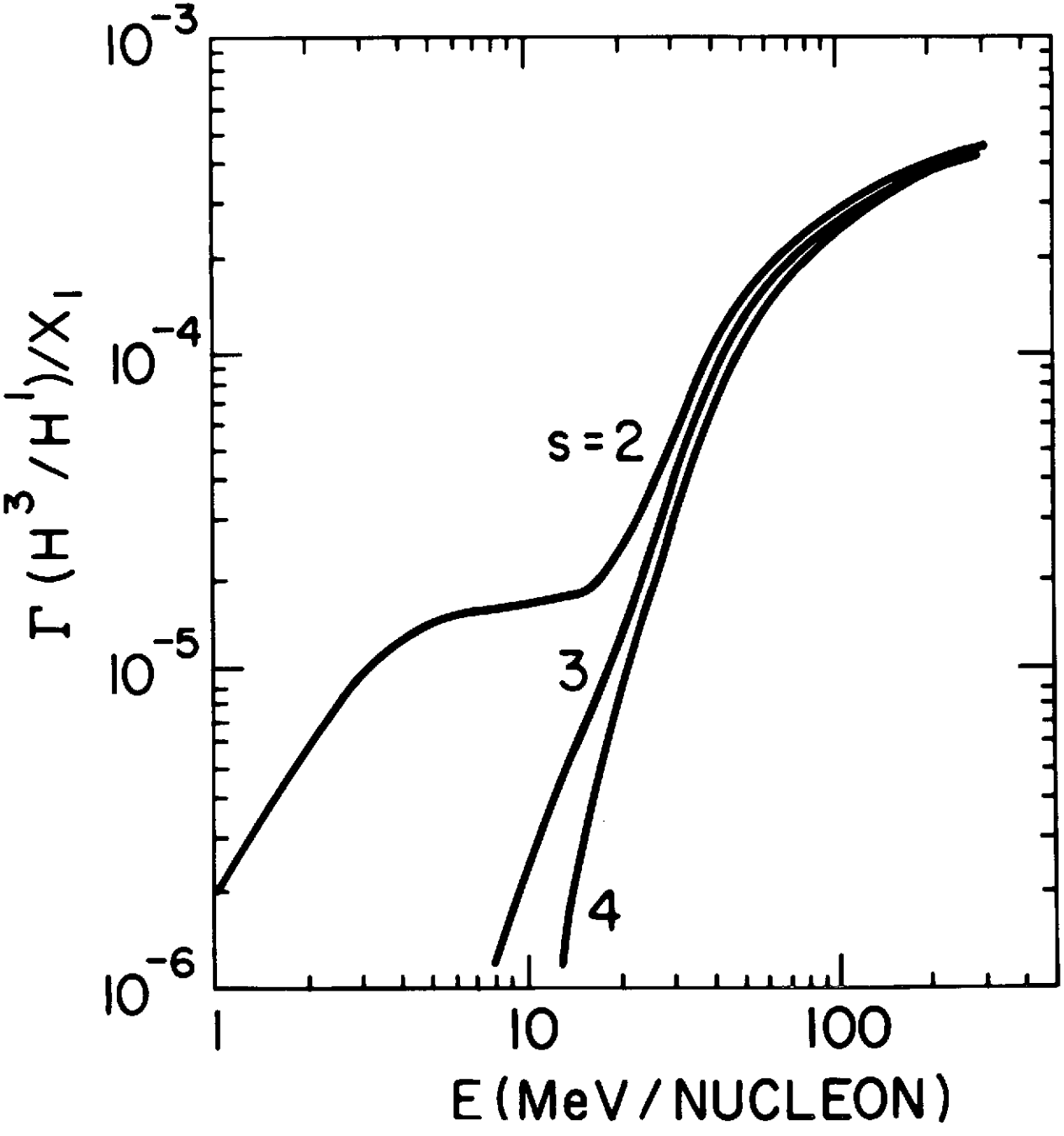

Figure 11

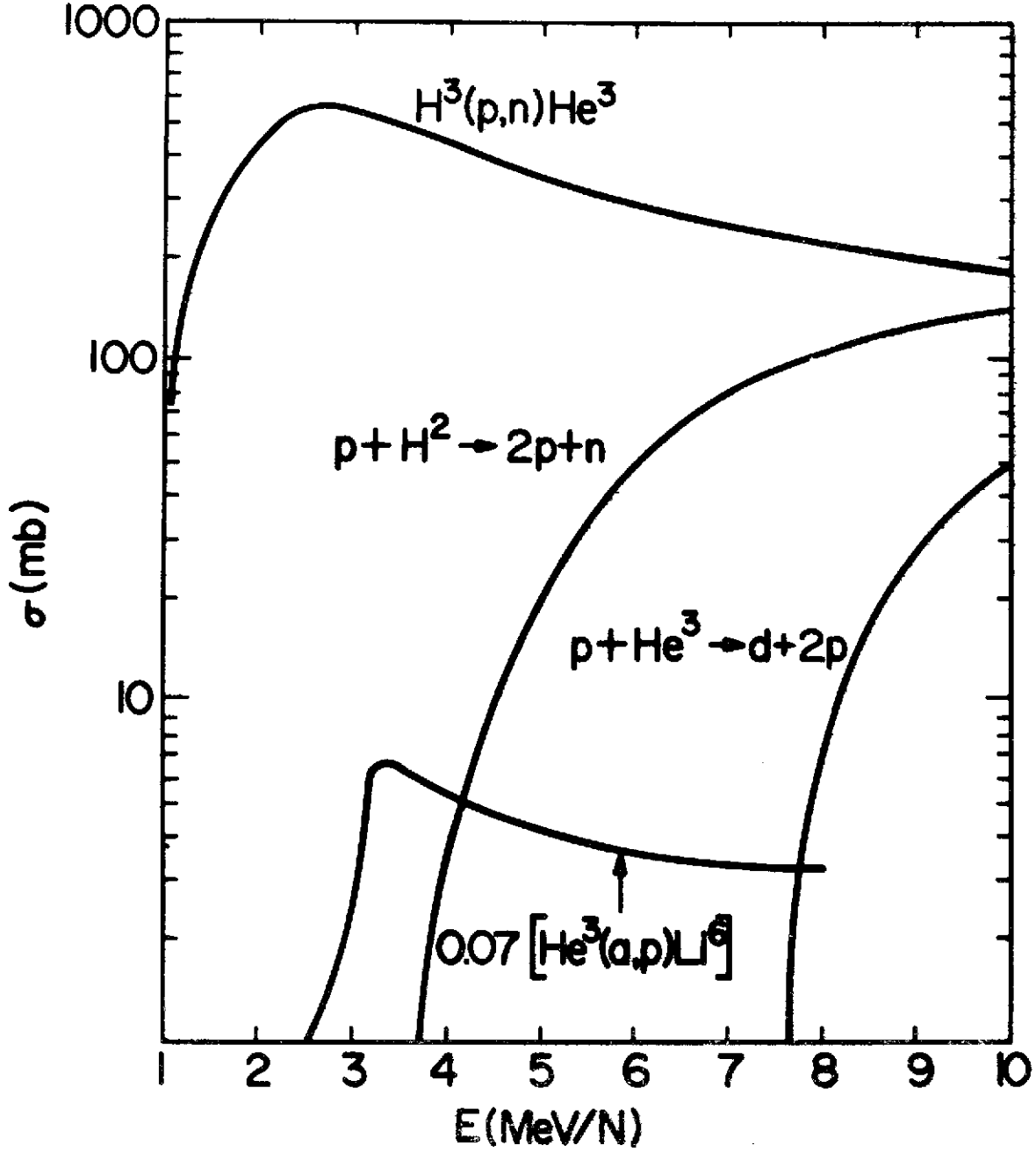

Figure 12

NASA–GSFC